

GAN-Leaks: A Taxonomy of Membership Inference Attacks against GANs

Dingfan Chen¹

Ning Yu^{2,3}

Yang Zhang¹

Mario Fritz¹

¹*CISPA Helmholtz Center for Information Security, Germany*

²*Max Planck Institute for Informatics, Germany*

³*University of Maryland, College Park*

{dingfan.chen, zhang, fritz}@cispa.saarland

ningyu@mpi-inf.mpg.de

Abstract

In recent years, the success of deep learning has carried over from discriminative models to generative models. In particular, generative adversarial networks (GANs) have facilitated a new level of performance ranging from media manipulation to dataset re-generation. Despite the success, the potential risks of privacy breach stemming from GANs are less well explored. In this paper, we focus on membership inference attack against GANs that has the potential to reveal information about victim models' training data. Specifically, we present the first taxonomy of membership inference attacks, which encompasses not only existing attacks but also our novel ones. We also propose the first generic attack model that can be instantiated in various settings according to adversary's knowledge about the victim model. We complement our systematic analysis of attack vectors with a comprehensive experimental study, that investigates the effectiveness of these attacks w.r.t. model type, training configurations, and attack type across three diverse application scenarios ranging from images, over medical data to location data. We show consistent effectiveness in all the setups, which bridges the assumption gap and performance gap in previous study with a complete spectrum of performance across settings. We conclusively remind users to think over before publicizing any part of their models.

1 Introduction

In the past few years, two categories of deep learning techniques have made tremendous achievements over machine learning tasks. The discriminative model has been successfully adopted in various prediction tasks, such as image recognition [39, 51, 74, 78], speech recognition [36, 42], machine translation [15, 24], computer-aided disease diagnosis [7, 72], etc. The generative model, on the other hand, has also gained increasing attention in recent years and has delivered appealing applications including photorealistic image synthesis [35, 54, 63], image editing [34, 45, 89], text generation [11, 84], sound generation [59, 61], etc. Most of such

applications are supported by either the generative adversarial networks (GANs) [10, 20, 35, 37, 47, 66, 70] or Variational AutoEncoder (VAE) [49, 67, 87], which decently improve synthesized media quality without leaving obvious artifacts.

In order to resonate the growing trend of deep learning in real business, many IT companies do not only embed deep learning models into their services to better market customers or understand business operations, but also commercialize deep learning itself as a service. They provide users with platforms where users can define their own deep learning tasks and apply the learned models, e.g., Google Prediction API [3], Amazon Machine Learning [1], Microsoft Azure Machine Learning [4], and BigML [2].

However, with the prevalence of online deep learning APIs, data privacy violation frequently happened due to data misuse with an inappropriate legal basis, e.g., the misuse of National Health Service data in the DeepMind project [5]. Data privacy can also be challenged by malicious users who intend to infer the original training data. The resulting privacy breach would raise serious issues because training data either contains sensitive attributes (e.g., a patient's disease history) or is cumbersome to collect. One such attack is membership inference [13, 31, 38, 69, 73] which aims to identify if a query data record was used to train a deep learning model. Overfitting to training data is the major cause for the feasibility of membership inference, as the learned model tends to memorize training inputs and perform better on them.

There are two main motivations for conducting research in membership inference attack. The first motivation is to validate and quantify the privacy vulnerability of a deep learning model. For models against which inference attacks are effective, owners can consider restricting their availability so as also to avoid other mounted attacks (e.g., profiling [65] or property inference [12, 60]). The second motivation is to establish wrongdoing, where, e.g., regulators can be clued from membership inference to propose the suspicion that a model was trained on personal data without an adequate legal basis [5].

Membership inference against discriminative deep learning

models has been largely explored [9, 13, 21, 43, 57, 60, 73, 88], while inference against generative models is still an open question. This is more challenging from the adversary side because the victim model does not directly provide confidence values about the overfitting of data records. Recently, Hayes et al. [38] present a first approach targeting GANs, which proposes to retrain a local copy of GAN in a black-box setting and to check the discriminator’s confidence for membership inference in a white-box setting. Their intuition is that the overfitting of a victim GAN is either incorporated in its discriminator or can be mimicked from a local copy of the discriminator. Hilprecht et al. [41] extend membership inference attack to both GANs and VAE via Monte Carlo integration [62]. Their intuition is that an overfitted generator tends to output data samples closer to the training data than to unseen data.

However, neither of them provides a complete, comprehensive, and practical analysis of membership inference attacks against GANs. For example, Hayes et al. [38] does not consider the realistic situation where the discriminator in a well-trained GAN is usually not deployed for query. Hilprecht et al. [41] investigate on toy image datasets and does not involve white-box attack against GANs. That motivates our contributions along this direction towards a more systematic analysis.

1.1 Contributions

Taxonomy of membership inference attacks against GANs. We propose a pioneering study to categorize attack settings against GANs. Given increasing order of the amount of knowledge about victim GAN accessible to the adversary, the settings are benchmarked as (1) full black-box generator, (2) partial black-box generator, (3) white-box generator, and (4) accessible discriminator. In particular, two of the settings, the partial black-box and white-box settings, are newly identified for attack model design. We then establish the first taxonomy for the existing and proposed attacks. See Section 3, Table 1, and Figure 1 for details.

The first generic attack model across settings and its novel instantiated variants. We propose the first generic attack model applicable to all the settings. See Section 4.1. The instantiated attack variants in the partial black-box and white-box settings are also the first attempts. See Section 4.3 and 4.4. Their effectiveness in Section 5.4 and 5.5, with a complete spectrum of performance across settings, bridges the gap between the existing full black-box attacks in [38, 41] and discriminator-accessible attack in [38]. See experimental comparisons in Section 5.7. We remind users of the high risk of privacy breach to publish the generator or even the input interface to their generator.

Comprehensive analysis in each setting. We progressively investigate attacks in each setting in the increasing order of amount of knowledge to adversary. See Section 5.3

to 5.5. In each setting, our research spans several orthogonal dimensions including three datasets with diverse modalities (Section 5.1), five victim GAN models that were the state-of-the-art at their release time (Section 5.1), two ablation study w.r.t. GAN training configurations (Section 5.2), and attack performance changes according to attack calibration (Section 4.6 and 5.6) or differential privacy defense during GAN training (Section 5.8).

1.2 Organization

The rest of the paper is organized as the following. Section 2 reviews the related work in the fields including various generative models, and membership inference attack and defense techniques. Section 3 elaborates attack taxonomy, and Section 4 introduces our generic attack model and instantiated attack variants for each setting. In Section 5, we evaluate attack performance in those settings and compare to existing work. Section 6 concludes the paper.

2 Related work

Generative adversarial networks (GANs). A GAN framework [10, 20, 35, 37, 47, 66, 70] consists of two neural networks, a generator and a discriminator, which are trained in an adversarial manner to generate data approximating the training data distribution. The generator takes random noise (latent code) as input and generates samples in the same modality as training data, while the discriminator takes samples from both the generator and training dataset as input and is trained for differentiating the two sources. During training, the two networks compete and evolve to reach the game equilibrium, such that the generator learns to generate more and more realistic samples aiming at fooling the discriminator, while the discriminator learns to more and more accurately tell the two sources apart. During testing, the discriminator is usually removed from deployment. One insight of GAN is to avoid hand-crafted similarity metric of sample-wise self-supervision. Instead, the discriminator adversarially learns deep features for a distribution-wise similarity metric. Experimentally, the generator can learn to generate samples with more realistic details, in contrast to only low-frequency accuracy from other hand-crafted metrics which average over training dataset. Therefore, GANs have shown improved photorealism in image synthesis [17, 54, 92], translation [45, 93, 94], or manipulation [8, 79, 80].

On the other hand, because of the nature of excluding sample-wise supervision, GANs implicitly model data distribution without processing individual images. Therefore, GANs can also be employed to re-render new samples following the original distribution but without revealing individual samples. Privacy protection can thus be potentially achieved by releasing only the distribution instead of the raw data to the

public, e.g., GAN-based de-identification for sensitive human-centric data [19, 58, 85] or health data [25, 86]. Therefore, membership inference attack against GANs is naturally more challenging.

We choose PGGAN [47], WGANGP [37], DCGAN [66], and MEDGAN [25] as the victim models to be attacked by membership inference, considering their pleasing performances on generating images and other data representations.

Variational AutoEncoder (VAE). VAE is an alternative generative framework [49, 67, 87] consists of two neural networks, an encoder and a decoder, which are cascaded to reconstruct data with sample-wise loss. The encoder maps data into a latent space, while the decoder maps the encoded latent representation back to data reconstruction. VAE regularizes the encoder by imposing a prior (usually a standard normal distribution) over the latent distribution. The VAE loss is then composed of the reconstruction error and a prior regularization in the form of Kullback-Leibler divergence.

Hybrid generative model. GANs often suffer from mode collapse issue, i.e., failing to generate appearances relevant to some training samples, due to the lack of sample-wise supervision, while VAE often lacks flexible hallucination capability. Therefore, a hybrid model, VAEGAN [18, 52], is proposed to jointly train a VAE and a GAN, where the VAE decoder and the GAN generator are collapsed into one by sharing trainable parameters. The GAN discriminator is used to measure sample similarity. We choose VAEGAN [18] as the fifth victim model to be attacked by membership inference.

Membership inference attacks. Shokri et al. [73] specifies attacks against discriminative models by exploiting differences in the model’s response to inputs that were or were not seen during training. Hayes et al. [38] specifies attacks against GANs by retraining a local copy of the victim GAN and checking the discriminator’s response to inputs. The latter attack is more challenging because GAN naturally excludes to sample-wise supervision and the retrained local copy may not accurately detect overfitting of the original training data. We also study in this direction but leverage only the pretrained generator. Another concurrent study by Hilprecht et al. [41] extends the attack against both GANs and VAE using Monte Carlo integration, but they only show attack against GANs in a black-box setting.

Other privacy-related attacks include model inversion [32, 33, 88], model extraction [82], model attribution [90], and attacks against distributed deep learning systems [9, 43, 60]. None of them are designed to determine if an individual data record belongs to the original training set or not, and thus cannot directly adapt to our desired membership inference attack against generative models.

Membership inference defenses. Regularization-based defenses include weight normalization [71] and random dropout [77]. Weight normalization is to reparameterize the model weight vectors by decoupling the length of those

	Latent code	Generator	Discriminator
[38] full black-box	×	■	×
[41] full black-box	×	■	×
Our full black-box (Sec. 4.2)	×	■	×
Our partial black-box (Sec. 4.3)	✓	■	×
Our white-box (Sec. 4.4)	✓	□	×
[38] accessible discriminator	×	×	✓

Table 1: Taxonomy of attack settings against GANs over the previous work and ours. (×: without access; ✓: with access; ■: black-box; □: white-box). The settings are more and more knowledgeable to attackers from top to bottom.

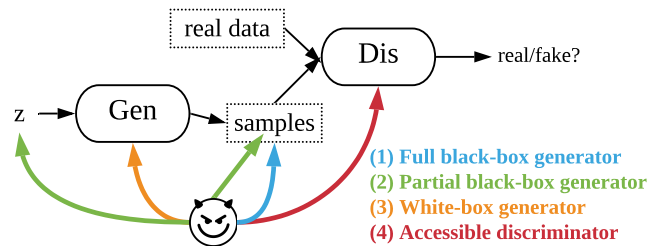


Figure 1: Taxonomy diagram of attack models against GANs. **Gen**: generator; **Dis**: discriminator; **z**: latent code input to the generator.

weights from their direction, and apply to all layers in both generator and discriminator in the victim model. Random dropout can be used to prevent overfitting by randomly zeroing connections between neurons during training.

Differential privacy defenses [16, 22, 23, 26–30, 75, 76, 83, 86, 95] are to inject carefully-sampled noise in either the forward passes or backward gradients during victim model training, so as to perturb data-related objective functions and thus mitigate inference attacks. We apply [29] in a variety of setups to analyze in which circumstances and to what extents it works.

3 Taxonomy of membership inference against GANs

In general, attack settings can be categorized into either white-box or black-box one. In the white-box setting, the victim network parameters are accessible to attackers, whereas in the black-box setting, they are unknown to attackers. Specifically to the attack against GANs, we further distinguish the settings based on the following criteria: (1) whether the discriminator is accessible or not, (2) whether the generator is white-box or black-box, and (3) whether the latent code of a generated sample is accessible or not. We categorize the existing and the proposed attacks in Table 1, and visualize different set-

tings in Figure 1. We elaborate each possible category in the following paragraphs in the **decreasing** order of the amount of knowledge to attackers.

Accessible discriminator. This is the most knowledgeable setting to attackers and it converts the attack against a GAN to the attack against a classical discriminative model, no matter whether the discriminator is white-box or black-box. Existing attack methods against discriminator models can be applied to this setting. For example, Shokri et al. [73] infer membership by checking the confidence value of the discriminator. This setting is also considered in [38], corresponding to the last row in Table 1. In practice, however, the discriminator of a well-trained GAN is usually discarded without being deployed to APIs, and thus not accessible to attackers. We, therefore, devote less effort to investigating the discriminator and mainly focus on the following practical settings where the attackers only have access to the generator.

White-box generator. This is the most knowledgeable setting to attackers when the discriminator of a GAN is no longer accessible. Attackers have access to the parameters of the generator. This is a realistic open-source scenario where users publish their well-trained generator without releasing the underlying training data. This scenario is also commonly studied in the community of differential privacy [29]. However, this is a novel setting for membership inference attack against GANs, which is not explored in [38] or [41]. It corresponds to the second last row in Table 1 and Section 4.4.

Partial black-box generator (known input-output pair). This is a less knowledgeable setting to attackers where they have no access to the parameters of the generator but have access to the latent code of each generated sample. This is also a realistic scenario where attackers submit their latent code as input and collect corresponding generated samples from the generator. This is another novel setting and not considered in [38] or [41]. It corresponds to the third last row in Table 1 and Section 4.3.

Full black-box generator (known output only). This is the least knowledgeable setting to attackers where they are unable to provide input but just blindly query samples from the well-trained black-box generator. This corresponds to the practical scenario of closed-source GAN-based APIs. Hayes et al. [38] investigate attacks in this setting by retraining a local copy of the API. Hilprecht et al. [41] sample data from the generator and use Monte Carlo approximation to score each query based on an elaborated design of distance metric between the query and the generated samples. Our idea is similar in spirit to Hilprecht et al. [41] but we design a low-skill attack method with a simpler implementation (Section 4.2) that achieves comparable or better performance (Section 5.3). Our attack and theirs correspond to the third, second, and first rows in Table 1, respectively.

Notation	Description
\mathcal{G}_v	Victim generator
\mathcal{A}	Attacker
\mathcal{R}	Attacker’s reconstructor
x	Query sample
z	Latent code (input to the generator)
D_{train}	Training set of the victim generator
\mathcal{G}_r	Attacker’s reference generator, described in Section 4.6

Table 2: Notations.

4 Membership inference attack against GANs

We first describe our generic attack model in Section 4.1, which applies to all the settings. Based on that, we introduce three attack variants under different settings from Section 4.2 to 4.4, respectively. Since our attack depends on sample distance metric, we elaborate our metric design in Section 4.5. Finally, we propose an attack calibration method in Section 4.6 to mitigate the relevance between our inference prediction and the generation difficulty of individual queries.

4.1 Generic attack model

We first summarize the notations used in the paper in Table 2. We formulate the membership inference attack as a binary classification task where we threshold the reconstruction error between a query sample x and its reconstructed copy $\mathcal{R}(x|\mathcal{G}_v)$ from the well-trained victim generator \mathcal{G}_v . Our intuition is that, given access to a generator, we should reconstruct samples better if they belong to the GAN training set, no matter how simple or difficult of those query samples. Mathematically,

$$\mathcal{A}(x|\mathcal{G}_v) \Rightarrow \begin{cases} x \in D_{\text{train}} & \text{if } L(x, \mathcal{R}(x|\mathcal{G}_v)) < \epsilon \\ x \notin D_{\text{train}} & \text{else} \end{cases} \quad (1)$$

where $L(\cdot, \cdot)$ is a distance metric between two samples and is elaborated in Section 4.5 and 4.6, and ϵ is a pre-defined threshold. See Figure 2(a) for a diagram.

The attacker’s goal is then to design \mathcal{R} such that it activates the most accurate possible performance of \mathcal{G}_v to approximate a query sample. In the following sections, we instantiate variants of \mathcal{R} for different attack settings in the **increasing** order of the amount of knowledge to attackers.

4.2 Full black-box attack

We start with the least knowledgeable setting where an attacker only has access to a black-box generator \mathcal{G}_v . The attacker is allowed no other operation but blindly collecting k samples from \mathcal{G}_v , denoted as $\{\mathcal{G}_v(\cdot)_i\}_{i=1}^k$. $\mathcal{G}_v(\cdot)$ indicates that the attacker has neither access nor control over latent code

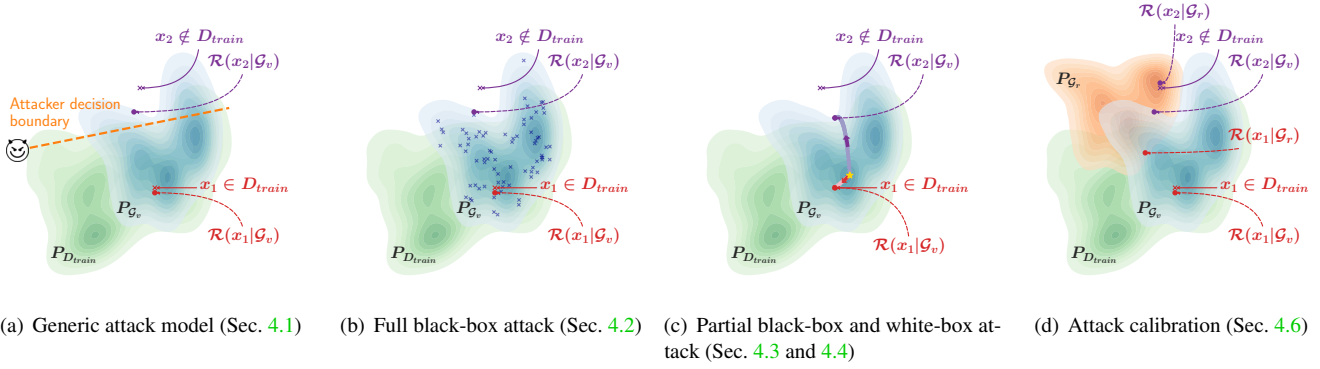


Figure 2: Diagram of our attacks. Mathematical notations refer to Table 2. P represents data distribution. The attacker’s goal is to infer if query samples x_1 and x_2 are members of real dataset D_{train} which is used to train G_v . A high-quality G_v approximates training data distribution very well so that P_{G_v} should be close enough to $P_{D_{\text{train}}}$. That enables attacks based on P_{G_v} . x_1 is a member of D_{train} so that it should be better represented by G_v with a smaller distance to its reconstructed copy $R(x_1|G_v)$. x_2 is not a member of D_{train} so that it should have a larger distance to its nearest neighbor $R(x_2|G_v)$ in P_{G_v} . An attacker in (a) just needs a decision boundary based on such a reconstruction distance to infer membership. In (b) the nearest neighbor is determined by sampling from P_{G_v} while in (c) it is done by optimization on the manifold of P_{G_v} . In (d) P_{G_r} is a third-party reference GAN distribution where the reconstruction distance is calibrated by subtracting the distance between x and $R(x|G_r)$. See Section 4 for more details.

input. We then define the reconstruction of x as the nearest neighbor from $\{G_v(\cdot)_i\}_{i=1}^k$. Mathematically,

$$\mathcal{R}(x|G_v) = \arg \min_{\hat{x} \in \{G_v(\cdot)_i\}_{i=1}^k} L(x, \hat{x}) \quad (2)$$

See Figure 2(b) for a diagram. Larger k leads to better reconstruction while sacrificing computation efficiency. Given a limited budget, we fix k to 20k throughout the experiments.

4.3 Partial black-box attack

Due to the curse of dimensionality, random samples in the black-box attack are sparsely distributed in the high dimensional space. The blind nearest neighbor search without considering the latent code input z may fail to find an accurate reconstruction. As the access to z is permitted in the partial black-box setting, we propose to establish attack exploiting z .

Concretely, the attacker performs an optimization w.r.t. z in order to accurately reconstruct the query samples x . Mathematically,

$$\mathcal{R}(x|G_v) = G_v(z^*) \quad (3)$$

where

$$z^* = \arg \min_z L(x, G_v(z)) \quad (4)$$

See Figure 2(c) for a diagram. Without knowing the parameters of G_v , the optimization is not differentiable and no gradient information is available. As only the evaluation of function (forward-pass through the generator) is allowed by the access of $\{z, G_v(z)\}$ pair, we propose to approximate the optimum via the Powell’s Conjugate Direction Method [64].

4.4 White-box attack

In the white-box setting, we have the same reconstruction formulation as in Section 4.3. See Figure 2(c) for a diagram. More advantageously to attackers, the reconstruction quality can be further boosted thanks to access to the parameters of G_v . This is because the optimization becomes differentiable with gradient backpropagation w.r.t. z , which can be more accurately solved by advanced first-order optimization algorithms, namely Adam [48], RMSPROP [81], and L-BFGS [55]. We tried all the three in our ablation study and found L-BFGS performs the best in terms of convergence rate.

4.5 Distance metric

Our baseline distance metric $L_{\text{base}}(\cdot, \cdot)$ consists of three terms: the element-wise (pixel-wise) difference term L_2 targets low-frequency components, the deep image feature term L_{lpips} (i.e., the Learned Perceptual Image Patch Similarity (LPIPS) metric [91]) targets realism details, and the regularization term penalizes latent code far from the prior distribution. Mathematically,

$$L_{\text{base}}(x, G_v(z)) = \lambda_1 L_2(x, G_v(z)) + \lambda_2 L_{\text{lpips}}(x, G_v(z)) + \lambda_3 L_{\text{reg}}(z) \quad (5)$$

where

$$L_2(x, G_v(z)) = \|x - G_v(z)\|_2^2 \quad (6)$$

$$L_{\text{reg}}(z) = (\|z\|_2^2 - \dim(z))^2 \quad (7)$$

λ_1 , λ_2 and λ_3 are used to enable/disable and balance the order of magnitude of each loss term, the values of which depend

on experiment configurations. For non-image data, $\lambda_2 = 0$ because LPIPS is no longer applicable. For full black-box attack, $\lambda_3 = 0$ because z is not accessible by the attacker.

4.6 Attack calibration

We noticed that the reconstruction error is query-dependent, i.e., some query samples are more difficult to reconstruct due to their intrinsically more complicated representations. In this case, the reconstruction error is dominated by the representations rather than by the membership clues. We, therefore, propose to mitigate the query dependency by first training a reference GAN \mathcal{G}_r with another disjoint dataset, and then calibrating our base reconstruction error according to the reference reconstruction error. Mathematically,

$$L(x, \mathcal{G}_v(z)) = L_{\text{base}}(x, \mathcal{G}_v(z)) - L_{\text{base}}(x, \mathcal{G}_r(z)) \quad (8)$$

The optimization on the well-trained \mathcal{G}_r is the same as on \mathcal{G}_v . See Figure 2(d) for a diagram.

5 Experiments

We discuss the experimental setup in Section 5.1. We propose two dimensions of ablation study in Section 5.2. From Section 5.3 to 5.5, we evaluate our attacks in three settings. We present the attack performance gain from calibration in Section 5.6. In Section 5.7, we compare with three baseline attack models. Finally, we investigate the effectiveness of one popular privacy defense scheme against our attack in various settings in Section 5.8.

5.1 Setup

Datasets. Hilprecht et al. [41] limit their investigations on low-resolution toy image datasets, e.g., MNIST [53] and CIFAR-10 [50]. We push our attack scenarios towards realism by conducting experiments on three modalities of datasets covering images, medical records, and location check-ins, which are considered with a high risk of privacy breach.

CelebA [56] is a large-scale face attributes dataset with 200k RGB images. Images are aligned to each other based on facial landmarks, which benefits GAN performance. We select at most 20k images, center-crop them, and resize them to 64×64 before GAN training.

MIMIC-III [46] is a public Electronic Health Records (EHR) database containing medical records of 46,520 intensive care unit (ICU) patients. We follow the same procedure as in [25] to pre-process the data, where each patient is represented by a 1071-dimension binary feature vector. We filter out patients with repeated vector presentations and yield 41,307 unique samples.

Instagram New-York [14] contains Instagram users’ check-ins at various locations in New York at different time stamps

	PG GAN	WGAN- GP	DC- GAN	VAE- GAN	SOTA ref	PGGAN w/ DP
FID	14.86	24.26	35.40	53.08	7.40	15.63

Table 3: FID for different GAN models trained on CelebA. “SOTA ref” represents the state-of-the-art result reported in [20] over 128×128 ImageNet ILSVRC 2012 dataset [68]. “w/ DP” represents the GAN model with DP privacy protection [6] (see Section 5.8).

from 2013 to 2017. We filter out users with less than 100 check-ins and yield 34,336 remaining samples. For sample representation, we first select 2,024 evenly-distributed time stamps. We then concatenate the longitude and latitude values of the check-in location at each time stamp, and yield a 4048-dimension vector for each sample. The longitude and latitude values are either retrieved from the dataset or linearly interpolated from the available neighboring time stamps. We then perform zero-mean normalization before GAN training.

Victim GAN models. We choose PGGAN [47], WGANGP [37], DCGAN [66], MEDGAN [25], and VAEGAN [18] into the victim model set, considering their pleasing performance on generating images and/or other data representations. We only train a subset of GAN models that are applicable for each dataset.

It is important to guarantee the high quality of well-trained GANs because attackers are more likely to target high-quality GANs with practical effectiveness. We noticed previous work [38, 41] only shows qualitative results of their victim GANs. In particular, Hayes et al. [38] did not show visually pleasing generation on the Labeled Faces in the Wild (LFW) dataset [44]. It may result from the mismatch between the dataset and their GAN models. Rather, we present better qualitative results of different GANs on CelebA (Figure 3), and further present the corresponding quantitative evaluation in terms of Fréchet Inception Distance (FID) metric [40] (Table 3). A smaller FID indicates the generated image set is more realistic and closer to real-world data distribution. We show that our GAN models are in a reasonable range from the state of the art.

Attack evaluation. The proposed membership inference attack is formulated as a binary classification given a threshold ϵ in Equation 1. Through varying ϵ , we measure the area under the receiver operating characteristic curve (AUCROC) to evaluate the attack performance. ROC reflects the relation between false-positive rate and true-positive rate given varying thresholds for a binary classification task and is robust to class imbalance. With a value range of $[0, 1]$, a larger AUCROC indicates a higher true-positive rate in a variety of thresholding, and thus better classification (attack) performance.

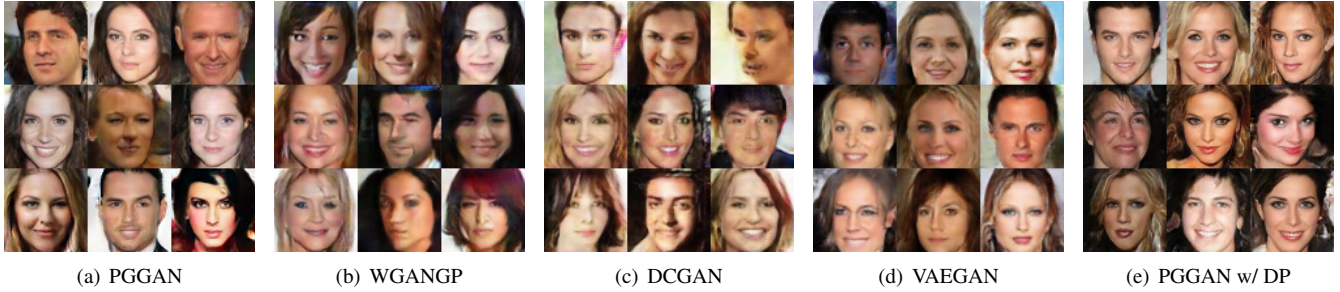


Figure 3: Generated images from different victim GAN models trained on CelebA.

5.2 Ablation study

We first list two dimensions of ablation study across attack settings. There are also some other dimensions specifically on the white-box attack, which is elaborated in Section 5.5.

GAN training set size. Training set size is highly related to the degree of overfitting of GAN training. A GAN model trained with a smaller size tends to more easily memorize individual training images and is thus more vulnerable to membership inference attack. Therefore, we evaluate the attack performance w.r.t. training set size. We exclude DCGAN and VAEGAN from evaluation since they yield unstable training for small training sets.

Random v.s. identity-based selection for GAN training set. There are different levels of difficulty for membership inference attack. For example, CelebA contains person identity information and we can design attack difficulty by composing GAN training set based on identity or not. In one case, we include all images of the selected individuals for training. In the other case, we ignore identity information and randomly select images for training. The former case is relatively easier to attackers with a larger margin between membership image set and non-membership image set. Therefore, we evaluate these two kinds of training set selection schemes on CelebA.

5.3 Evaluation on full black-box attack

We start with evaluating our preliminary low-skill black-box attack model in order to gain a sense of the difficulty of the whole problem.

Performance w.r.t. GAN training set size. Figure 4(a) to 4(c) plot the attack performance against different GAN models on the three datasets. The attack performs sufficiently well when the training set is small for all three datasets. For instance, on CelebA, when the training set contains up to 512 images, attacker’s AUCROC on both PGGAN and WGANGP are above 0.95. This indicates an almost perfect attack and a serious privacy breach. For larger training sets, however, the attacks become less effective as the degree of overfitting decreases and GAN’s capability shifts from memorization

to hallucination. That reminds users to collect more data for GAN training in order to reduce privacy breach for each individual sample. Moreover, PGGAN becomes more vulnerable than WGANGP on CelebA when the training size becomes larger. WGANGP is consistently more vulnerable than MEDGAN on MIMIC-III regardless of training size.

Performance w.r.t. GAN training set selection. Figure 5(a) shows the comparisons against four victim GAN models. We find that, consistently, all the GAN models are more vulnerable when the training set is selected based on identity. That reminds users to pay more attention to identity-based privacy breach, which is more likely to happen than instance-based privacy breach. Moreover, DCGAN and VAEGAN are more resistant against full black-box attack with AUCROC only marginally above 0.5 (random guess baseline). The resistance order is inversely correlated to the generation quality order of GANs in Tabel 3. That reminds users that a better GAN performance is at the cost of a higher privacy breach risk.

5.4 Evaluation on partial black-box attack

We then equip attackers with more knowledge to perform partial black-box attack.

Performance w.r.t. GAN training set selection. Figure 5(b) shows the comparison on four victim GAN models. We find that all models become more vulnerable to identity-based selection. Still, DCGAN is the most resistant victim against membership inference in both training set selection schemes.

Comparison to full black-box attack. Comparing between Figure 5(a) and 5(b), the attack performance against each GAN model consistently and significantly improves from black-box setting to partial black-box setting, which reminds users not to provide the input interface to unauthorized ones.

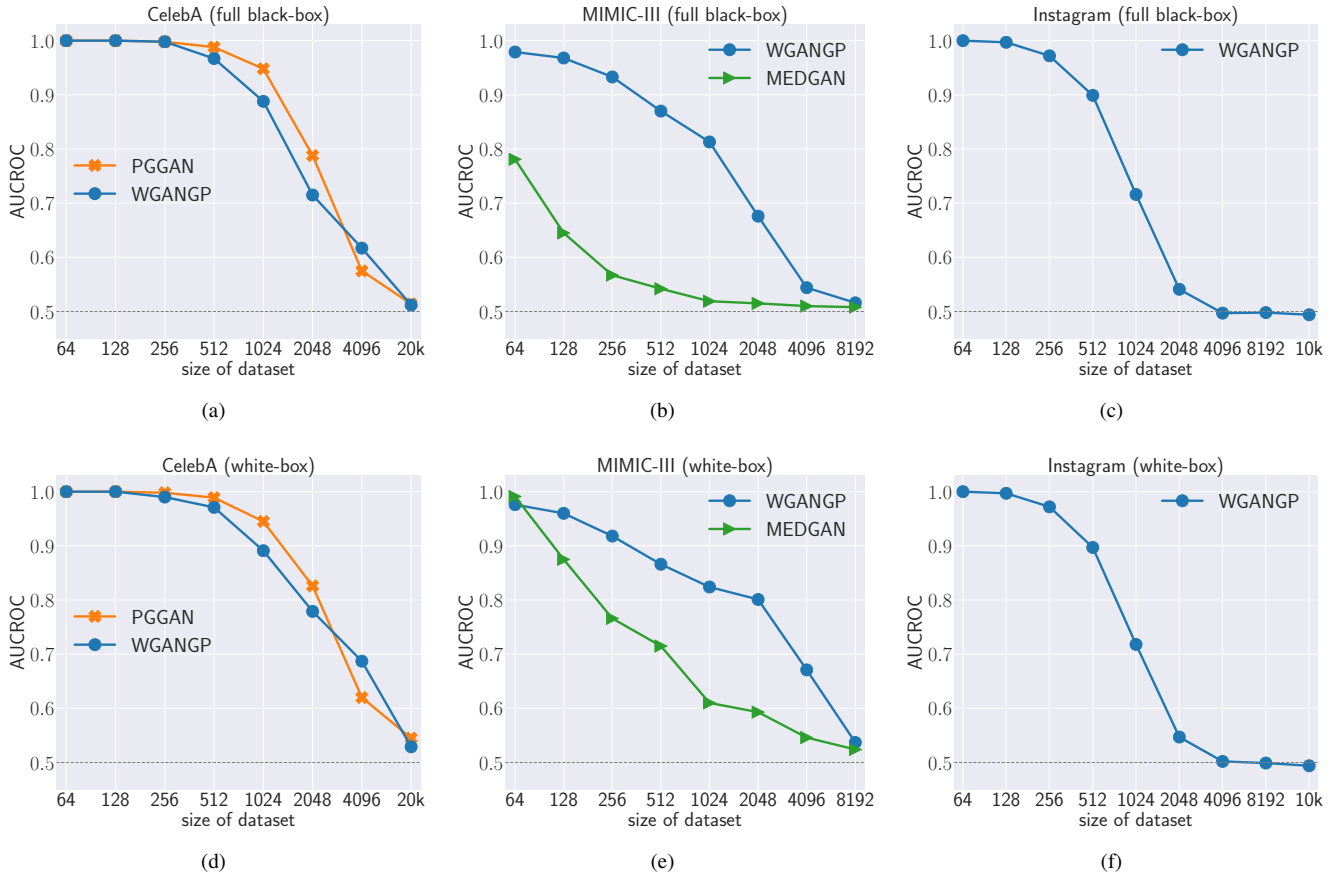


Figure 4: Full black-box attack (the first row) and white-box attack (the second row) performance w.r.t. GAN training set size. See Table 6 and Table 9 in Appendix for quantitative results.

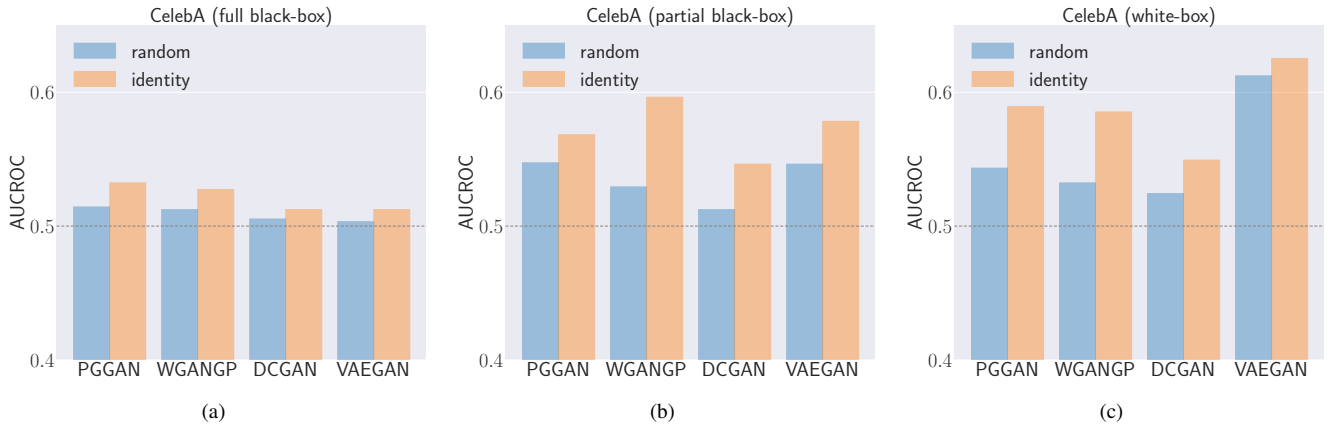


Figure 5: Attack performance on the random v.s. identity-based GAN training set selection. We only focus on CelebA across attack settings. See Table 7 in Appendix for quantitative results.

5.5 Evaluation on white-box attack

We further equip attackers with access to the parameters of the generator to perform white-box attack. As the optimization in

white-box attack involves more technical details, we conduct additional ablation study and sanity check in this setting.

Ablation on optimization initialization. Due to the non-convexity of our optimization problem, the choice of ini-

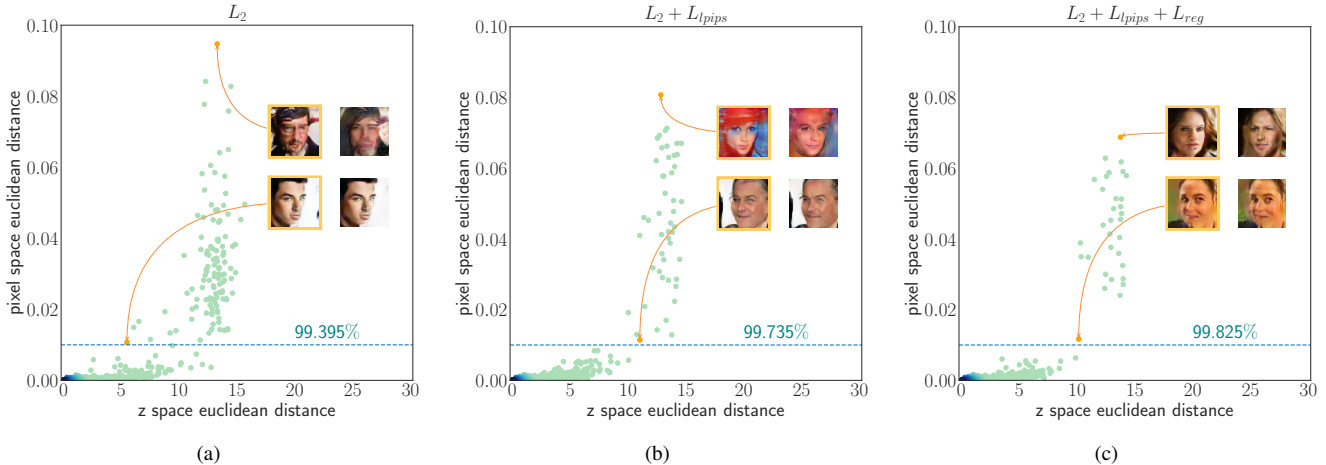


Figure 6: Reconstruction error plots of PGGAN-generated samples on CelebA. The x-axis represents the Euclidean distance between a reconstructed latent code to its ground truth value. The y-axis represents the L_2 residual in the image domain. The images in orange frame are generated samples. Their reconstructed copies are shown on their right. Samples below the dashed line have reconstruction residuals smaller than 0.01, where no visual difference can be observed. Therefore, the reconstruction is in general better if there is a higher portion of sample points below the dashed line (a higher successful reconstruction rate). (a) Reconstruction results when disabling L_{lipips} and L_{reg} ($\lambda_1 = 1.0, \lambda_2 = 0, \lambda_3 = 0$). (b) Reconstruction results when disabling L_{reg} ($\lambda_1 = 1.0, \lambda_2 = 0.2, \lambda_3 = 0$). (c) Reconstruction results when enabling all the L_2, L_{lipips} and L_{reg} terms ($\lambda_1 = 1.0, \lambda_2 = 0.2, \lambda_3 = 0.001$). We find that using all the terms most benefits the reconstruction.

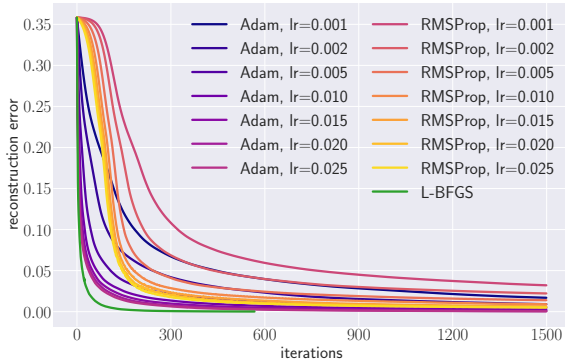


Figure 7: Convergence rate of various optimizers (Adam, RMSProp, L-BFGS) with different learning rates. Mean initialization ($z_0 = \mu$) is applied in this ablation study.

tialization is of great importance. We explore three different initialization heuristics in our experiments, including mean ($z_0 = \mu$), random ($z_0 \sim \mathcal{N}(\mu, \Sigma)$), and nearest neighbour ($z_0 = \operatorname{argmin}_{z \in \{z_i\}_{i=1}^k} \|\mathcal{G}_v(z) - x\|_2^2$). We find that the mean and nearest neighbor initialization perform well in practice, and are in general better than random initialization in terms of the successful reconstruction rate (reconstruction error smaller than 0.01). Therefore, we apply the mean and nearest neighbor initialization in parallel, and choose the one with smaller reconstruction error for the attack.

Ablation on optimization method. We explore three optimizers with a range of hyper-parameter search: Adam [48],

	DCGAN	PGGAN	WGANGP	VAEGAN
Success rate (%)	99.89	99.83	99.55	99.25

Table 4: Successful reconstruction rate for generated samples from different GANs.

RMSProp [81], and L-BFGS [55] for reconstructing generated samples of PGGAN on CelebA. Figure 7 shows that L-BFGS achieves superior convergence rate with no additional hyper-parameter. Therefore, we select L-BFGS as our default optimizer in the white-box setting.

Ablation on distance metric design for optimization. We show the effectiveness of our objective design (Equation 5). Although optimizing only for element-wise term L_2 yields reasonably good reconstruction in most cases, we observe undesired blur in reconstruction for CelebA images. Incorporating deep image feature term L_{lipips} and regularization term L_{reg} benefits the successful reconstruction rate. See Figure 6 for a demonstration.

Sanity check on distance metric design for optimization. In addition, we check if the non-convexity of our objective function affects the feasibility of attack against different victim GANs. We apply optimization to reconstruct generated samples. Ideally, the reconstruction should have no error because the query samples are directly generated by the model, i.e., their preimages exist. We set a threshold of 0.01 to the reconstruction error for counting successful reconstruction rate, and evaluate the success rate for four GAN models trained

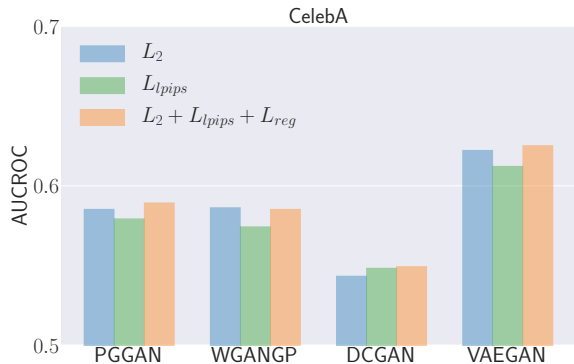


Figure 8: White-box attack performance against various GANs on CelebA, w.r.t. distance metric design for classification. See Table 8 in Appendix for quantitative results.

on CelebA. Table 4 shows that we obtained more than 99% success rate for all the GANs, which verifies the feasibility of our optimization-based attack.

Ablation on distance metric design for classification.

We propose to enable/disable λ_1 , λ_2 , or λ_3 in Equation 5 to investigate the contribution of each term towards classification thresholding (membership inference) on CelebA. In detail, we consider using (1) the element-wise difference term L_2 only, (2) the deep image feature term L_{lpips} only, and (3) all the three terms together to evaluate attack performance. Figure 8 shows the AUCROC of attack against each various GANs. We find that our complete distance metric design achieves general superiority to single terms. Therefore, we use the complete distance metric for classification thresholding.

Moreover, the attack is less effective against DCGAN while more effective against VAEGAN. The success in attacking VAEGAN can be explained by the sample-wise self-supervision during VAEGAN training, which enforces to memorize training data. Therefore, we argue that combining VAE and GAN may alleviate mode collapse but at the cost of higher privacy breach risk.

Performance w.r.t. GAN training set size. Figure 4(d) to 4(f) plot the attack performance against different GAN models on the three datasets. We find that the attack becomes less effective as the training set becomes larger, similar to that in the black-box setting. For CelebA, the attack remains effective for 20k training samples, while for MIMIC-III and Instagram, this number decreases to 8192 and 2048, respectively. The strong similarity between the member and non-member in these two non-image datasets increases the difficulty for attack, which explains the deteriorated performance.

Performance w.r.t. GAN training set selection. Figure 5(c) shows the comparisons against four victim GAN models. Our attack is much more effective when we compose GAN training set according to identity, which is similar to those in the full and partial black-box settings.

Comparison to full and partial black-box attacks. For membership inference attack, it is an important question whether or to what extent the white-box attack is more effective than the black-box ones. We find that against GAN models the white-box attack is much more effective. Comparisons across subfigures in Figure 5 show that the AUCROC values increase by at least 0.03 when changing from full black-box to white-box setting. Compared to the partial black-box attack, the white-box attack achieves noticeably better performance against PGGAN and VAEGAN. Moreover, conducting white-box attack requires much less time cost than conducting partial black-box attack. Therefore, we conclude that providing users with model parameters (white-box setting) does incur high privacy breach risk.

5.6 Performance gain from attack calibration

We perform calibration on all the settings. Especially for full and partial black-box settings, attackers do not have prior knowledge on victim model architectures. We thus train a PGGAN on LFW face dataset [44] and use it as the generic reference model for calibrating all victim models trained on CelebA. Similarly, for MIMIC-III, we use WGANGP as the reference model for MedGAN and vice versa. In other words, we have to guarantee that our calibrated attacks strictly follow the black-box assumption.

Figure 9 compares attack performance on CelebA before and after applying calibration. The AUCROC values are improved consistently across all the GAN architectures in all the settings. In general, the white-box attack calibration yields the greatest performance gain. Moreover, the improvement is especially significant when attacking against VAEGAN, as the AUCROC value increases by 0.2 after applying calibration.

Figure 10 compares attack performance on the other two non-image datasets. The performance is also consistently boosted for all training set sizes after calibration.

5.7 Comparison to baseline attacks

We compare our calibrated attack to two recent membership inference attack baselines: Hayes et al. [38] (denoted as LOGAN) and Hilprecht et al. [41] (denoted as MC, standing for their proposed Monte Carlo sampling method). As described in our taxonomy (Section 3), LOGAN includes a full black-box attack model and a discriminator-accessible attack model against GANs. The latter is regarded as the most knowledgeable but unrealistic setting because the discriminator in GAN is usually not accessible in practice. But we still compare to both settings for the completeness of our taxonomy and experiments. MC includes a full black-box attack model but does not include a white-box attack model against GANs. Their white-box attack model is only targeting VAE. We thus only compare to their former model. Note that, to the best of our

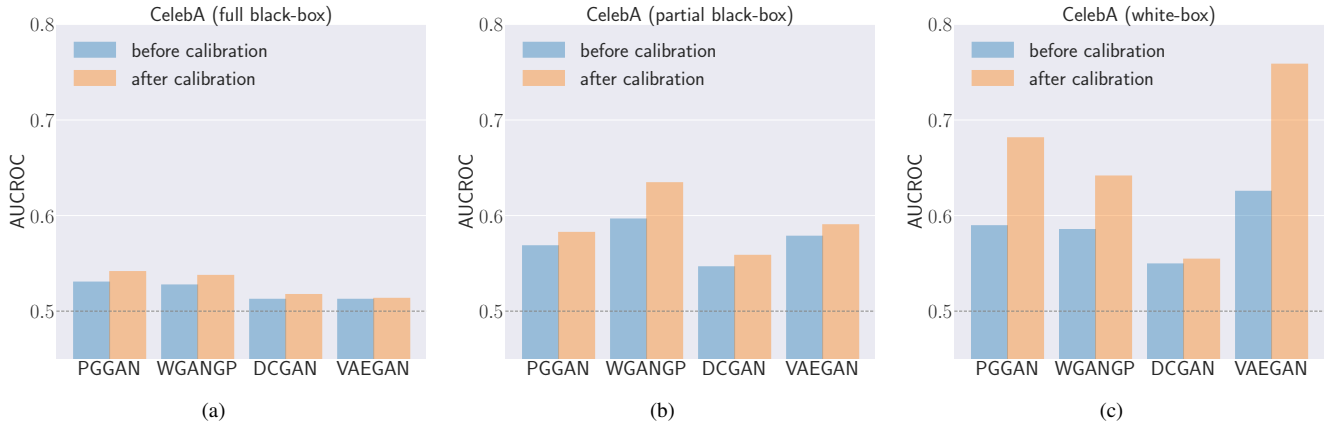


Figure 9: Attack performance before and after calibration on CelebA. See Table 10 in Appendix for quantitative results.

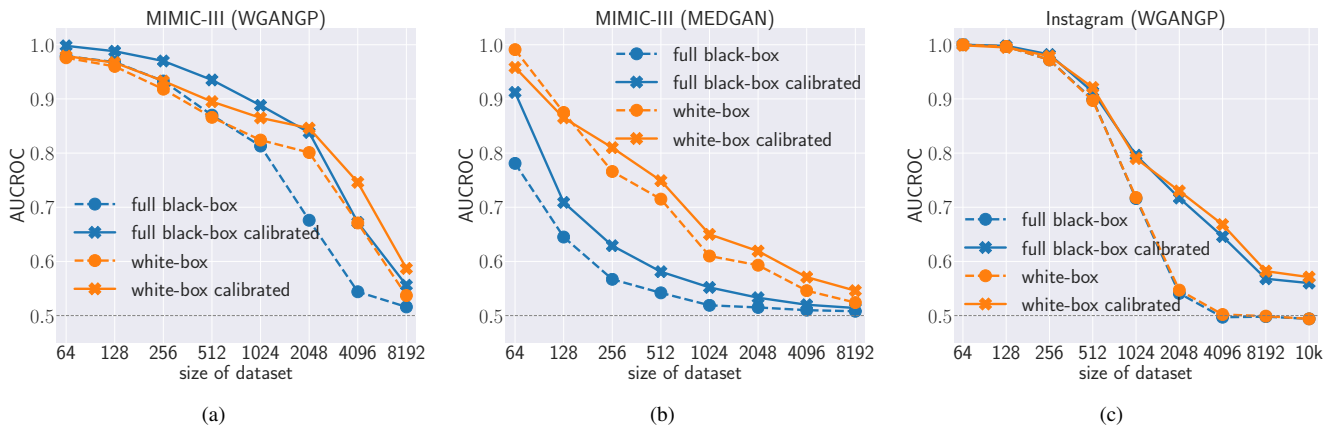


Figure 10: Attack performance before and after calibration for non-image datasets w.r.t. GAN training set sizes. See Table 11 in Appendix for quantitative results.

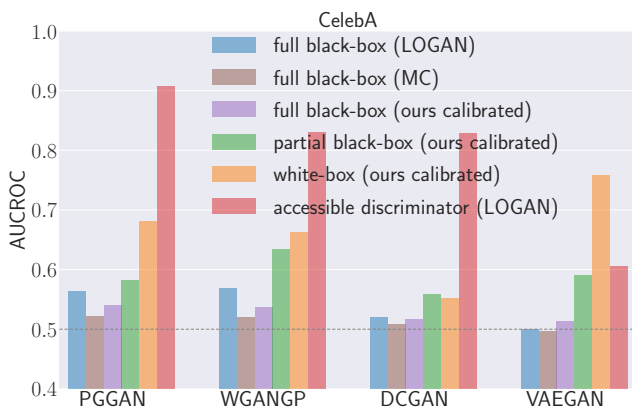


Figure 11: Comparison of different attacks on CelebA. See Table 12 in Appendix for quantitative results.

knowledge, there does not exist another attack against GANs

in the partial black-box or white-box settings.

Figure 11 and 12 show the comparisons, considering several datasets, victim GAN models, and GAN training set sizes, and across different settings. We skip MC on the non-image datasets as it is not directly applicable in terms of their distance calculation. Our findings are as follow.

In black-box setting, our low-skill attack consistently outperforms MC and outperforms LOGAN on the non-image datasets. It also achieves comparable performance to LOGAN on CelebA but with a much simpler implementation.

Our white-box and even partial black-box attacks consistently outperform the other full black-box attacks, which reminds users that the release of the generator or even just the input to the generator can lead to severe risk of privacy breach. With a complete spectrum of performance across settings, they bridge the performance gap between LOGAN black-box attack and LOGAN discriminator-accessible attack.

LOGAN with access to the discriminator is the most effective attack, except when against VAEGAN. The effectiveness

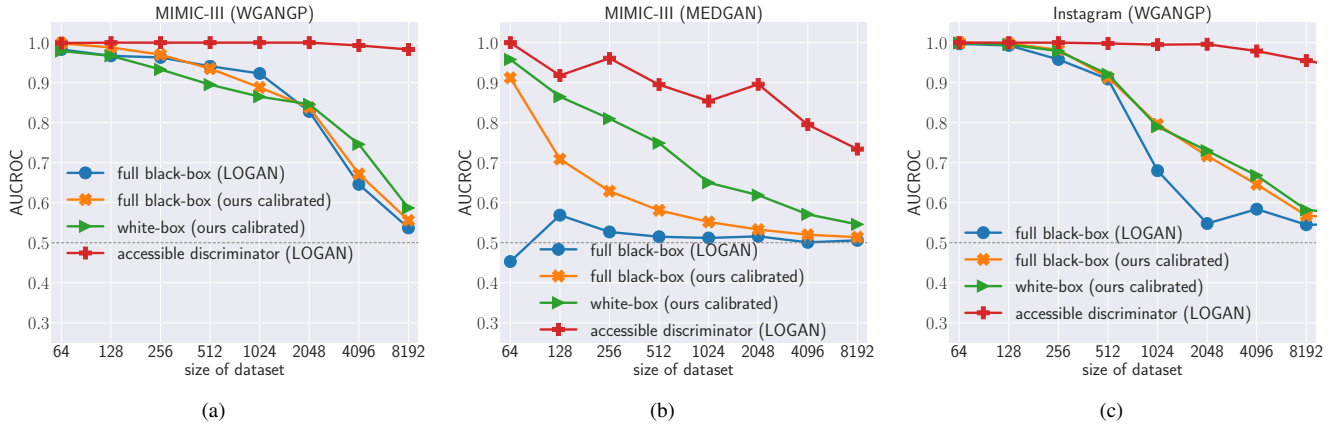


Figure 12: Comparison of different attacks on the other two non-image datasets w.r.t. GAN training set size. See Table 13 in Appendix for quantitative results.

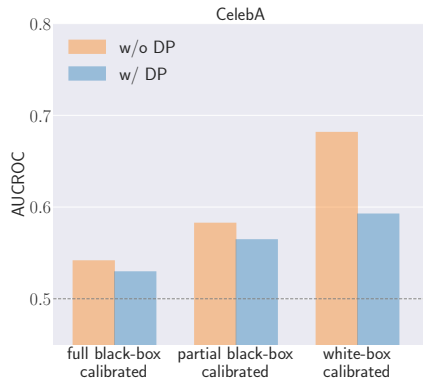


Figure 13: Attack performance against PGGAN on CelebA with or without DP defense. See Table 14 in Appendix for quantitative results.

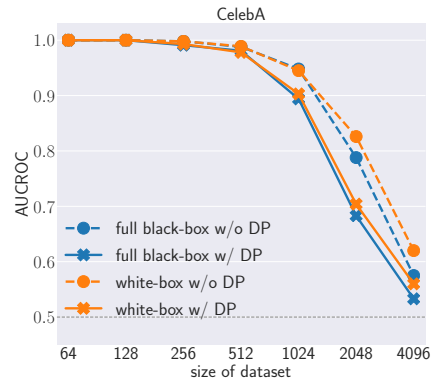


Figure 14: Attack performance against PGGAN on CelebA with or without DP defense, w.r.t. GAN training set size. See Table 15 in Appendix for quantitative results.

can be explained by the fact that the discriminator is explicitly trained to maximize the margin between training set (membership samples) and generated set (a subset of non-membership samples), which eventually yields very accurate confidence scores for membership inference. However, the discriminator score is not very effective against VAEGAN because its training relies more on sample-wise supervision than on the adversarial loss. Although this is not a fair comparison due to the more knowledgeable assumption, it reminds users of the exceptional risk of publishing the discriminator.

5.8 Defense

We investigate one popular defense mechanism against membership inference attack, i.e., the differential private (DP) stochastic gradient descent [6]. The algorithm can be summarized into two steps. First, the per-sample gradient computed

at each training iteration is clipped by its L_2 norm with a pre-defined threshold. Second, random noise is added to this gradient in order to protect privacy. The noisy gradient is then used for gradient descent optimization. In this scheme, however, privacy protection is at the cost of computational complexity and utility deterioration, i.e., slower training and lower generation quality.

We conduct attacks against PGGAN on CelebA, which has been defended by DP. We skip the other cases because DP always deteriorates generation quality to an unacceptable level. The DP hyper-parameters are selected through the grid search. We fix the norm threshold to 1.0 and the noise scale to 10^{-4} .

Figure 13 and 14 depict the attack performance in different settings. We observe a consistent decrease in AUCROC in all the settings. Therefore, DP is effective in general against our attack. However, applying DP into training leads to a

much higher computation cost ($10\times$ slower) in practice due to the per-sample gradient modification. Moreover, DP results in a deterioration of GAN utility, which is witnessed by an increasing FID (comparing the last and second columns in Table 3). Moreover, for obtaining a pleasing level of utility, the noise scale has to be limited to a small value, which, in turn, cannot defend membership inference attack completely. For example, for all the settings, our attack still achieves better performance than the random guess baseline (AUCROC = 0.5).

6 Conclusion

We have established the first taxonomy of membership inference attacks against GANs, with which we hope to benchmark research in this direction in the future. We have also proposed the first generic attack model based on reconstruction, that is applicable to all the settings according to the amount of attacker’s knowledge about the victim model. In particular, the instantiated attack variants in the partial black-box and white-box settings are our another novelty to bridge the assumption and performance gap in the previous work [38, 41]. Comprehensive experiments show consistent effectiveness and a complete spectrum of performance in a variety of setups spanning three datasets, five victim GAN models, two directions of ablation study, attack calibration, as well as differential privacy defense, which conclusively remind users to be careful about releasing any part of their models.

References

- [1] Amazon machine learning. <https://aws.amazon.com/machine-learning>.
- [2] Bigml. <https://bigml.com>.
- [3] Google prediction api. <https://cloud.google.com/prediction>.
- [4] Microsoft azure machine learning. <https://studio.azureml.net>.
- [5] The guardian view on google’s nhs grab: legally inappropriate. <https://news.sky.com/story/google-received-1-6-million-nhs-patients-data-on-an-inappropriate-legal-basis-10879142>, 2017.
- [6] Martin Abadi, Andy Chu, Ian Goodfellow, H Brendan McMahan, Ilya Mironov, Kunal Talwar, and Li Zhang. Deep learning with differential privacy. In *Proceedings of the 2016 ACM SIGSAC Conference on Computer and Communications Security*, pages 308–318. ACM, 2016.
- [7] Filippo Amato, Alberto López, Eladia María Peña-Méndez, Petr Vaňhara, Aleš Hampl, and Josef Havel. Artificial neural networks in medical diagnosis, 2013.
- [8] Grigory Antipov, Moez Baccouche, and Jean-Luc Dugelay. Face aging with conditional generative adversarial networks. In *Image Processing, 2017 IEEE International Conference on*, pages 2089–2093. IEEE, 2017.
- [9] Yoshinori Aono, Takuya Hayashi, Lihua Wang, Shiho Moriai, et al. Privacy-preserving deep learning: Revisited and enhanced. In *International Conference on Applications and Techniques in Information Security*, pages 100–110. Springer, 2017.
- [10] Martin Arjovsky, Soumith Chintala, and Léon Bottou. Wasserstein generative adversarial networks. In *International Conference on Machine Learning*, pages 214–223, 2017.
- [11] Sanjeev Arora, Rong Ge, Yingyu Liang, Tengyu Ma, and Yi Zhang. Generalization and equilibrium in generative adversarial nets (gans). In *Proceedings of the 34th International Conference on Machine Learning-Volume 70*, pages 224–232. JMLR. org, 2017.
- [12] Giuseppe Ateniese, Giovanni Felici, Luigi V Mancini, Angelo Spognardi, Antonio Villani, and Domenico Vitali. Hacking smart machines with smarter ones: How to extract meaningful data from machine learning classifiers. *arXiv preprint arXiv:1306.4447*, 2013.
- [13] Michael Backes, Pascal Berrang, Mathias Humbert, and Praveen Manoharan. Membership privacy in microrna-based studies. In *Proceedings of the 2016 ACM SIGSAC Conference on Computer and Communications Security*, pages 319–330. ACM, 2016.
- [14] Michael Backes, Mathias Humbert, Jun Pang, and Yang Zhang. walk2friends: Inferring social links from mobility profiles. In *Proceedings of the 2017 ACM SIGSAC Conference on Computer and Communications Security*, pages 1943–1957. ACM, 2017.
- [15] Dzmitry Bahdanau, Kyunghyun Cho, and Yoshua Bengio. Neural machine translation by jointly learning to align and translate. *arXiv preprint arXiv:1409.0473*, 2014.
- [16] Brett K Beaulieu-Jones, Zhiwei Steven Wu, Chris Williams, and Casey S Greene. Privacy-preserving generative deep neural networks support clinical data sharing. *bioRxiv*. DOI, 10:159756, 2017.
- [17] Urs Bergmann, Nikolay Jetchev, and Roland Vollgraf. Learning texture manifolds with the periodic spatial gan. In *Proceedings of the 34th International Conference on Machine Learning-Volume 70*, pages 469–477. JMLR. org, 2017.

- [18] Apratim Bhattacharyya, Bernt Schiele, and Mario Fritz. Accurate and diverse sampling of sequences based on a “best of many” sample objective. In *IEEE Conference on Computer Vision and Pattern Recognition*, 2018.
- [19] Karla Brkic, Ivan Sikiric, Tomislav Hrkac, and Zoran Kalafatic. I know that person: Generative full body and face de-identification of people in images. In *2017 IEEE Conference on Computer Vision and Pattern Recognition Workshops*, pages 1319–1328. IEEE, 2017.
- [20] Andrew Brock, Jeff Donahue, and Karen Simonyan. Large scale GAN training for high fidelity natural image synthesis. In *International Conference on Learning Representations*, 2019.
- [21] Nicholas Carlini, Chang Liu, Jernej Kos, Úlfar Erlingsson, and Dawn Song. The secret sharer: Measuring unintended neural network memorization & extracting secrets. *arXiv preprint arXiv:1802.08232*, 2018.
- [22] Kamalika Chaudhuri and Claire Monteleoni. Privacy-preserving logistic regression. In *Advances in Neural Information Processing Systems*, pages 289–296, 2009.
- [23] Kamalika Chaudhuri, Claire Monteleoni, and Anand D Sarwate. Differentially private empirical risk minimization. *Journal of Machine Learning Research*, 12(Mar):1069–1109, 2011.
- [24] Kyunghyun Cho, Bart Van Merriënboer, Caglar Gulcehre, Dzmitry Bahdanau, Fethi Bougares, Holger Schwenk, and Yoshua Bengio. Learning phrase representations using rnn encoder-decoder for statistical machine translation. *arXiv preprint arXiv:1406.1078*, 2014.
- [25] Edward Choi, Siddharth Biswal, Bradley Malin, Jon Duke, Walter F Stewart, and Jimeng Sun. Generating multi-label discrete patient records using generative adversarial networks. *arXiv preprint arXiv:1703.06490*, 2017.
- [26] Irit Dinur and Kobbi Nissim. Revealing information while preserving privacy. In *Proceedings of the Twenty-Second ACM SIGMOD-SIGACT-SIGART Symposium on Principles of Database Systems*, pages 202–210. ACM, 2003.
- [27] C Dwork. Differential privacy: a survey of results. In *International Conference on Theory and Applications of Models of Computation (pp. 1–19)*. Springer, Berlin Heidelberg, 2008.
- [28] Cynthia Dwork. Differential privacy [g]?? automata, languages and programming. *ser: Lecture Notes in Computer Scienc*, 4052:112, 2006.
- [29] Cynthia Dwork, Frank McSherry, Kobbi Nissim, and Adam Smith. Calibrating noise to sensitivity in private data analysis. In *Theory of Cryptography Conference*, pages 265–284. Springer, 2006.
- [30] Cynthia Dwork and Kobbi Nissim. Privacy-preserving datamining on vertically partitioned databases. In *Annual International Cryptology Conference*, pages 528–544. Springer, 2004.
- [31] Cynthia Dwork, Adam Smith, Thomas Steinke, Jonathan Ullman, and Salil Vadhan. Robust traceability from trace amounts. In *2015 IEEE 56th Annual Symposium on Foundations of Computer Science*, pages 650–669. IEEE, 2015.
- [32] Matt Fredrikson, Somesh Jha, and Thomas Ristenpart. Model inversion attacks that exploit confidence information and basic countermeasures. In *Proceedings of the 22nd ACM SIGSAC Conference on Computer and Communications Security*, pages 1322–1333. ACM, 2015.
- [33] Matthew Fredrikson, Eric Lantz, Somesh Jha, Simon Lin, David Page, and Thomas Ristenpart. Privacy in pharmacogenetics: An end-to-end case study of personalized warfarin dosing. In *23rd {USENIX} Security Symposium ({USENIX} Security 14)*, pages 17–32, 2014.
- [34] Leon A Gatys, Alexander S Ecker, and Matthias Bethge. Image style transfer using convolutional neural networks. In *Proceedings of the IEEE Conference on Computer Vision and Pattern Recognition*, pages 2414–2423, 2016.
- [35] Ian Goodfellow, Jean Pouget-Abadie, Mehdi Mirza, Bing Xu, David Warde-Farley, Sherjil Ozair, Aaron Courville, and Yoshua Bengio. Generative adversarial nets. In *Advances in Neural Information Processing Systems*, pages 2672–2680, 2014.
- [36] Alex Graves, Abdel-rahman Mohamed, and Geoffrey Hinton. Speech recognition with deep recurrent neural networks. In *2013 IEEE International Conference on Acoustics, Speech and Signal Processing*, pages 6645–6649. IEEE, 2013.
- [37] Ishaan Gulrajani, Faruk Ahmed, Martin Arjovsky, Vincent Dumoulin, and Aaron C Courville. Improved training of wasserstein gans. In *Advances in Neural Information Processing Systems*, pages 5767–5777, 2017.
- [38] Jamie Hayes, Luca Melis, George Danezis, and Emiliano De Cristofaro. Logan: Membership inference attacks against generative models. *Proceedings on Privacy Enhancing Technologies*, 2019(1):133–152, 2019.

- [39] Kaiming He, Xiangyu Zhang, Shaoqing Ren, and Jian Sun. Deep residual learning for image recognition. In *Proceedings of the IEEE Conference on Computer Vision and Pattern Recognition*, pages 770–778, 2016.
- [40] Martin Heusel, Hubert Ramsauer, Thomas Unterthiner, Bernhard Nessler, and Sepp Hochreiter. Gans trained by a two time-scale update rule converge to a local nash equilibrium. In *Advances in Neural Information Processing Systems*, pages 6626–6637, 2017.
- [41] Benjamin Hilprecht, Martin Härterich, and Daniel Bernau. Monte carlo and reconstruction membership inference attacks against generative models. *Proceedings on Privacy Enhancing Technologies*, 2019(4):232–249, 2019.
- [42] Geoffrey Hinton, Li Deng, Dong Yu, George Dahl, Abdel-rahman Mohamed, Navdeep Jaitly, Andrew Senior, Vincent Vanhoucke, Patrick Nguyen, Brian Kingsbury, et al. Deep neural networks for acoustic modeling in speech recognition. *IEEE Signal Processing Magazine*, 29, 2012.
- [43] Briland Hitaj, Giuseppe Ateniese, and Fernando Perez-Cruz. Deep models under the gan: information leakage from collaborative deep learning. In *Proceedings of the 2017 ACM SIGSAC Conference on Computer and Communications Security*, pages 603–618. ACM, 2017.
- [44] Gary B. Huang, Manu Ramesh, Tamara Berg, and Erik Learned-Miller. Labeled faces in the wild: A database for studying face recognition in unconstrained environments. Technical Report 07-49, University of Massachusetts, Amherst, October 2007.
- [45] Phillip Isola, Jun-Yan Zhu, Tinghui Zhou, and Alexei A Efros. Image-to-image translation with conditional adversarial networks. In *Proceedings of the IEEE Conference on Computer Vision and Pattern Recognition*, pages 1125–1134, 2017.
- [46] Alistair EW Johnson, Tom J Pollard, Lu Shen, H Lehman Li-wei, Mengling Feng, Mohammad Ghassemi, Benjamin Moody, Peter Szolovits, Leo Anthony Celi, and Roger G Mark. Mimic-iii, a freely accessible critical care database. *Scientific Data*, 3:160035, 2016.
- [47] Tero Karras, Timo Aila, Samuli Laine, and Jaakko Lehtinen. Progressive growing of GANs for improved quality, stability, and variation. In *International Conference on Learning Representations*, 2018.
- [48] Diederik P Kingma and Jimmy Ba. Adam: A method for stochastic optimization. In *International Conference on Learning Representations*, 2014.
- [49] Diederik P Kingma and Max Welling. Auto-encoding variational bayes. In *International Conference on Learning Representations*, 2014.
- [50] Alex Krizhevsky, Geoffrey Hinton, et al. Learning multiple layers of features from tiny images. Technical report, Citeseer, 2009.
- [51] Alex Krizhevsky, Ilya Sutskever, and Geoffrey E Hinton. Imagenet classification with deep convolutional neural networks. In *Advances in Neural Information Processing Systems*, pages 1097–1105, 2012.
- [52] Anders Boesen Lindbo Larsen, Søren Kaae Sønderby, Hugo Larochelle, and Ole Winther. Autoencoding beyond pixels using a learned similarity metric. In Maria Florina Balcan and Kilian Q. Weinberger, editors, *Proceedings of The 33rd International Conference on Machine Learning*, volume 48 of *Proceedings of Machine Learning Research*, pages 1558–1566, New York, New York, USA, 20–22 Jun 2016. PMLR.
- [53] Yann LeCun, Corinna Cortes, and CJ Burges. Mnist handwritten digit database. *AT&T Labs [Online]*. Available: <http://yann.lecun.com/exdb/mnist>, 2:18, 2010.
- [54] Chuan Li and Michael Wand. Precomputed real-time texture synthesis with markovian generative adversarial networks. In *European Conference on Computer Vision*, pages 702–716. Springer, 2016.
- [55] Dong C Liu and Jorge Nocedal. On the limited memory bfgs method for large scale optimization. *Mathematical Programming*, 45(1-3):503–528, 1989.
- [56] Ziwei Liu, Ping Luo, Xiaogang Wang, and Xiaoou Tang. Deep learning face attributes in the wild. In *Proceedings of International Conference on Computer Vision*, December 2015.
- [57] Yunhui Long, Vincent Bindschaedler, Lei Wang, Diyue Bu, Xiaofeng Wang, Haixu Tang, Carl A Gunter, and Kai Chen. Understanding membership inferences on well-generalized learning models. *arXiv preprint arXiv:1802.04889*, 2018.
- [58] Blaž Meden, Refik Can Mallı, Sebastjan Fabijan, Hazım Kemal Ekenel, Vitomir Štruc, and Peter Peer. Face deidentification with generative deep neural networks. *IET Signal Processing*, 11(9):1046–1054, 2017.
- [59] Soroush Mehri, Kundan Kumar, Ishaan Gulrajani, Rithesh Kumar, Shubham Jain, Jose Sotelo, Aaron Courville, and Yoshua Bengio. Samplernn: An unconditional end-to-end neural audio generation model. In *International Conference on Learning Representations*, 2016.

- [60] Luca Melis, Congzheng Song, Emiliano De Cristofaro, and Vitaly Shmatikov. Exploiting unintended feature leakage in collaborative learning. *arXiv preprint arXiv:1805.04049*, 2018.
- [61] Aaron van den Oord, Sander Dieleman, Heiga Zen, Karen Simonyan, Oriol Vinyals, Alex Graves, Nal Kalchbrenner, Andrew Senior, and Koray Kavukcuoglu. Wavenet: A generative model for raw audio. *arXiv preprint arXiv:1609.03499*, 2016.
- [62] Art B Owen. Monte carlo theory, methods and examples. *Monte Carlo Theory, Methods and Examples*. Art Owen, 2013.
- [63] Deepak Pathak, Philipp Krahenbuhl, Jeff Donahue, Trevor Darrell, and Alexei A Efros. Context encoders: Feature learning by inpainting. In *Proceedings of the IEEE Conference on Computer Vision and Pattern Recognition*, pages 2536–2544, 2016.
- [64] M. J. D. Powell. An efficient method for finding the minimum of a function of several variables without calculating derivatives. *The Computer Journal*, 7(2):155–162, 01 1964.
- [65] Apostolos Pyrgelis, Carmela Troncoso, and Emiliano De Cristofaro. What does the crowd say about you? evaluating aggregation-based location privacy. *Proceedings on Privacy Enhancing Technologies*, 2017(4):156–176, 2017.
- [66] Alec Radford, Luke Metz, and Soumith Chintala. Unsupervised representation learning with deep convolutional generative adversarial networks. *arXiv preprint arXiv:1511.06434*, 2015.
- [67] Danilo Jimenez Rezende, Shakir Mohamed, and Daan Wierstra. Stochastic backpropagation and approximate inference in deep generative models. *arXiv preprint arXiv:1401.4082*, 2014.
- [68] Olga Russakovsky, Jia Deng, Hao Su, Jonathan Krause, Sanjeev Satheesh, Sean Ma, Zhiheng Huang, Andrej Karpathy, Aditya Khosla, Michael Bernstein, et al. Imagenet large scale visual recognition challenge. *International Journal of Computer Vision*, 115(3):211–252, 2015.
- [69] Ahmed Salem, Yang Zhang, Mathias Humbert, Pascal Berrang, Mario Fritz, and Michael Backes. ML-leaks: Model and data independent membership inference attacks and defenses on machine learning models. In *Proceedings of the 2019 Network and Distributed System Security Symposium*. Internet Society, 2019.
- [70] Tim Salimans, Ian Goodfellow, Wojciech Zaremba, Vicki Cheung, Alec Radford, and Xi Chen. Improved techniques for training gans. In *Advances in Neural Information Processing Systems*, pages 2234–2242, 2016.
- [71] Tim Salimans and Durk P Kingma. Weight normalization: A simple reparameterization to accelerate training of deep neural networks. In *Advances in Neural Information Processing Systems*, pages 901–909, 2016.
- [72] Hoo-Chang Shin, Holger R Roth, Mingchen Gao, Le Lu, Ziyue Xu, Isabella Nogues, Jianhua Yao, Daniel Mollura, and Ronald M Summers. Deep convolutional neural networks for computer-aided detection: Cnn architectures, dataset characteristics and transfer learning. *IEEE Transactions on Medical Imaging*, 35(5):1285–1298, 2016.
- [73] Reza Shokri, Marco Stronati, Congzheng Song, and Vitaly Shmatikov. Membership inference attacks against machine learning models. In *2017 IEEE Symposium on Security and Privacy (SP)*, pages 3–18. IEEE, 2017.
- [74] K. Simonyan and A. Zisserman. Very deep convolutional networks for large-scale image recognition. In *International Conference on Learning Representations*, 2015.
- [75] Shuang Song, Kamalika Chaudhuri, and Anand Sarwate. Learning from data with heterogeneous noise using sgd. In *Artificial Intelligence and Statistics*, pages 894–902, 2015.
- [76] Shuang Song, Kamalika Chaudhuri, and Anand D Sarwate. Stochastic gradient descent with differentially private updates. In *2013 IEEE Global Conference on Signal and Information Processing*, pages 245–248. IEEE, 2013.
- [77] Nitish Srivastava, Geoffrey Hinton, Alex Krizhevsky, Ilya Sutskever, and Ruslan Salakhutdinov. Dropout: a simple way to prevent neural networks from overfitting. *The Journal of Machine Learning Research*, 15(1):1929–1958, 2014.
- [78] Christian Szegedy, Wei Liu, Yangqing Jia, Pierre Sermanet, Scott Reed, Dragomir Anguelov, Dumitru Erhan, Vincent Vanhoucke, and Andrew Rabinovich. Going deeper with convolutions. In *Proceedings of the IEEE Conference on Computer Vision and Pattern Recognition*, pages 1–9, 2015.
- [79] Justus Thies, Michael Zollhöfer, Matthias Nießner, Levi Valgaerts, Marc Stamminger, and Christian Theobalt. Real-time expression transfer for facial reenactment. *ACM Trans. Graph.*, 34(6):183–1, 2015.

- [80] Justus Thies, Michael Zollhofer, Marc Stamminger, Christian Theobalt, and Matthias Nießner. Face2face: Real-time face capture and reenactment of rgb videos. In *Proceedings of the IEEE Conference on Computer Vision and Pattern Recognition*, pages 2387–2395, 2016.
- [81] Tijmen Tieleman and Geoffrey Hinton. Lecture 6.5-rmsprop: Divide the gradient by a running average of its recent magnitude. *COURSERA: Neural Networks for Machine Learning*, 4(2):26–31, 2012.
- [82] Florian Tramèr, Fan Zhang, Ari Juels, Michael K Reiter, and Thomas Ristenpart. Stealing machine learning models via prediction apis. In *25th {USENIX} Security Symposium ({USENIX} Security 16)*, pages 601–618, 2016.
- [83] Aleksei Triastcyn and Boi Faltings. Generating differentially private datasets using gans, 2018.
- [84] Oriol Vinyals, Alexander Toshev, Samy Bengio, and Dumitru Erhan. Show and tell: A neural image caption generator. In *Proceedings of the IEEE Conference on Computer Vision and Pattern Recognition*, pages 3156–3164, 2015.
- [85] Yifan Wu, Fan Yang, and Haibin Ling. Privacy-protective-gan for face de-identification. *arXiv preprint arXiv:1806.08906*, 2018.
- [86] Liyang Xie, Kaixiang Lin, Shu Wang, Fei Wang, and Jiayu Zhou. Differentially private generative adversarial network. *arXiv preprint arXiv:1802.06739*, 2018.
- [87] Xinchun Yan, Jimei Yang, Kihyuk Sohn, and Honglak Lee. Attribute2image: Conditional image generation from visual attributes. corr abs/1512.00570, 2015.
- [88] Samuel Yeom, Irene Giacomelli, Matt Fredrikson, and Somesh Jha. Privacy risk in machine learning: Analyzing the connection to overfitting. In *2018 IEEE 31st Computer Security Foundations Symposium*, pages 268–282. IEEE, 2018.
- [89] Ning Yu, Connelly Barnes, Eli Shechtman, Sohrab Amirghodsi, and Michal Lukáč. Texture mixer: A network for controllable synthesis and interpolation of texture. In *IEEE Conference on Computer Vision and Pattern Recognition*, 2019.
- [90] Ning Yu, Larry Davis, and Mario Fritz. Attributing fake images to gans: Learning and analyzing gan fingerprints. In *International Conference on Computer Vision (ICCV)*, 2019.
- [91] Richard Zhang, Phillip Isola, Alexei A Efros, Eli Shechtman, and Oliver Wang. The unreasonable effectiveness of deep features as a perceptual metric. In *Proceedings of the IEEE Conference on Computer Vision and Pattern Recognition*, pages 586–595, 2018.
- [92] Yang Zhou, Zhen Zhu, Xiang Bai, Dani Lischinski, Daniel Cohen-Or, and Hui Huang. Non-stationary texture synthesis by adversarial expansion. *ACM Trans. Graph.*, 37(4):49:1–49:13, 2018.
- [93] Jun-Yan Zhu, Taesung Park, Phillip Isola, and Alexei A Efros. Unpaired image-to-image translation using cycle-consistent adversarial networks. In *Proceedings of the IEEE International Conference on Computer Vision*, pages 2223–2232, 2017.
- [94] Jun-Yan Zhu, Richard Zhang, Deepak Pathak, Trevor Darrell, Alexei A Efros, Oliver Wang, and Eli Shechtman. Toward multimodal image-to-image translation. In *Advances in Neural Information Processing Systems*, 2017.
- [95] Tianqing Zhu, Gang Li, Wanlei Zhou, and S Yu Philip. Differentially private data publishing and analysis: A survey. *IEEE Transactions on Knowledge and Data Engineering*, 29(8):1619–1638, 2017.

Appendix

A Experiment setup

A.1 Hyper-parameter setting

We set $\lambda_1 = 1.0$, $\lambda_2 = 0.2$, $\lambda_3 = 0.001$ for our partial black-box and white-box attack on CelebA, and set $\lambda_1 = 1.0$, $\lambda_2 = 0.0$, $\lambda_3 = 0.0$ for the other cases. The maximum number of iterations for optimization are set to be 1000 for our white-box attack and 10 for our partial black-box attack.

A.2 Model architectures

We use the official implementations of the victim GAN models.¹ We re-implement WGAN-GP model with a fully-connected structure for non-image datasets. The network architecture is summarized in Table 5. The depth of both the generator and discriminator is set to 5. The dimension of the hidden layer is fix to be 512. We use ReLU as the activation function for the generator and Leaky ReLU with $\alpha = 0.2$ for the discriminator, except for the output layer where either the sigmoid or identity function is used.

Generator (MIMIC-III)	Generator (Instagram)	Discriminator (MIMIC-III and Instagram)
FC (512)	FC (512)	FC (512)
ReLU	ReLU	LeakyReLU (0.2)
FC (512)	FC (512)	FC (512)
ReLU	ReLU	LeakyReLU (0.2)
FC (512)	FC (512)	FC (512)
ReLU	ReLU	LeakyReLU (0.2)
FC (512)	FC (512)	FC (512)
ReLU	ReLU	LeakyReLU (0.2)
FC (dim(x))	FC (dim(x))	FC (1)
Sigmoid	Identity	Identity

Table 5: Network architecture of WGAN-GP on MIMIC-III and Instagram.

A.3 Implementation of baseline attacks

We provide more details of implementing baseline attacks that are discussed in Section 5.7.

LOGAN. For CelebA, we employ DCGAN as the attack model, which is the same as in the original paper [38]. For MIMIC-III and Instagram, we use WGAN-GP as the attack model.

MC. For implementing MC on CelebA, we apply the same process of their best attack on RGB image dataset: First, we employ principal component analysis (PCA) on a data subset disjoint from the query data. Then, we keep the first 120 PCA

¹ https://github.com/tkarras/progressive_growing_of_gans, https://github.com/igul222/improved_wgan_training, <https://github.com/carpedm20/DCGAN-tensorflow>, <https://github.com/mp2893/medgan>

components as suggested in the original paper [41] and apply dimensionality reduction on the generated and query data. Finally, we calculate the Euclidean distance of the projected data and use the median heuristic to choose the threshold for MC attack.

B Quantitative results

B.1 Evaluation on full black-box attack

Attack performance w.r.t. training set size. Table 6 corresponds to Figure 4(a), 4(b), and 4(c) in the main paper.

		(a) CelebA									
		64	128	256	512	1024	2048	4096	20k		
PGGAN		1.00	1.00	1.00	0.99	0.95	0.79	0.58	0.51		
WGAN-GP		1.00	1.00	1.00	0.97	0.89	0.72	0.62	0.51		
		(b) MIMIC-III									
		64	128	256	512	1024	2048	4096	8192		
WGAN-GP		0.98	0.97	0.93	0.87	0.81	0.68	0.54	0.52		
MEDGAN		0.78	0.65	0.57	0.54	0.52	0.52	0.51	0.51		
		(c) Instagram									
		64	128	256	512	1024	2048	4096	8192	10k	
WGAN-GP		1.00	1.00	0.97	0.90	0.72	0.54	0.50	0.50	0.50	

Table 6: Full black-box attack performance w.r.t. training set size.

Attack performance w.r.t. training set selection. Table 7 corresponds to Figure 5 in the main paper.

		(a) Full black-box			
		PGGAN	WGAN-GP	DCGAN	VAEGAN
random		0.51	0.51	0.51	0.50
identity		0.53	0.53	0.51	0.51
		(b) Partial black-box			
		PGGAN	WGAN-GP	DCGAN	VAEGAN
random		0.55	0.53	0.51	0.55
identity		0.57	0.60	0.55	0.58
		(c) White-box			
		PGGAN	WGAN-GP	DCGAN	VAEGAN
random		0.54	0.53	0.52	0.61
identity		0.59	0.59	0.55	0.63

Table 7: Attack performance on the random v.s. identity-based GAN training set selection. We only focus on CelebA across attack settings.

B.2 Evaluation on partial black-box attack

Attack performance w.r.t. training set selection. Table 7 corresponds to Figure 5 in the main paper.

B.3 Evaluation on white-box attack

Ablation on distance metric design for classification. Table 8 corresponds to Figure 8 in the main paper.

	DCGAN	PGGAN	WGANGP	VAEGAN
L_2	0.54	0.59	0.59	0.62
L_{lips}	0.55	0.58	0.57	0.61
$L_2 + L_{\text{lips}} + L_{\text{reg}}$	0.55	0.59	0.59	0.63

Table 8: White-box attack performance against various GANs on CelebA, w.r.t. distance metric design for classification.

Attack performance w.r.t. training set size. Table 9 corresponds to Figure 4(d), 4(e), and 4(f) in the main paper.

(a) CelebA									
	64	128	256	512	1024	2048	4096	8192	10k
PGGAN	1.00	1.00	1.00	0.99	0.95	0.83	0.62	0.55	
WGANGP	1.00	1.00	0.99	0.97	0.89	0.78	0.69	0.53	

(b) MIMIC-III									
	64	128	256	512	1024	2048	4096	8192	10k
WGANGP	0.98	0.96	0.92	0.87	0.82	0.80	0.67	0.54	
MEDGAN	0.99	0.88	0.77	0.72	0.61	0.59	0.55	0.52	

(c) Instagram									
	64	128	256	512	1024	2048	4096	8192	10k
WGANGP	1.00	1.00	0.97	0.90	0.72	0.55	0.50	0.50	0.49

Table 9: White-box attack performance w.r.t. training set size.

Attack performance w.r.t. training set selection. Table 7 corresponds to Figure 5 in the main paper.

B.4 Attack calibration

Table 10 corresponds to Figure 9 in the main paper. Table 11 corresponds to Figure 10 in the main paper.

(a) Full black-box				
	PGGAN	WGANGP	DCGAN	VAEGAN
before calibration	0.53	0.53	0.51	0.51
after calibration	0.54	0.54	0.52	0.51

(b) Partial black-box				
	PGGAN	WGANGP	DCGAN	VAEGAN
before calibration	0.57	0.60	0.55	0.58
after calibration	0.58	0.63	0.56	0.59

(c) White-box				
	PGGAN	WGANGP	DCGAN	VAEGAN
before calibration	0.59	0.59	0.55	0.63
after calibration	0.68	0.64	0.55	0.76

Table 10: Attack performance before and after calibration on CelebA.

(a) MIMIC-III (WGANGP)								
	64	128	256	512	1024	2048	4096	20k
full bb	0.98	0.97	0.93	0.87	0.81	0.68	0.54	0.52
full bb (calibrated)	1.00	0.99	0.97	0.94	0.89	0.84	0.67	0.56
wb	0.98	0.96	0.92	0.87	0.82	0.80	0.67	0.54
wb (calibrated)	0.98	0.97	0.93	0.90	0.87	0.85	0.75	0.59

(b) MIMIC-III (MEDGAN)								
	64	128	256	512	1024	2048	4096	8192
full bb	0.78	0.65	0.57	0.54	0.52	0.52	0.51	0.51
full bb (calibrated)	0.91	0.71	0.63	0.58	0.55	0.53	0.52	0.51
wb	0.99	0.88	0.77	0.72	0.61	0.59	0.55	0.52
wb (calibrated)	0.96	0.87	0.81	0.75	0.65	0.62	0.57	0.55

(c) Instagram (WGANGP)									
	64	128	256	512	1024	2048	4096	8192	10k
full bb	1.00	1.00	0.97	0.90	0.72	0.54	0.50	0.50	0.49
full bb (calibrated)	1.00	1.00	0.98	0.91	0.80	0.72	0.65	0.57	0.56
wb	1.00	1.00	0.97	0.90	0.72	0.55	0.50	0.50	0.49
wb (calibrated)	1.00	1.00	0.98	0.92	0.79	0.73	0.67	0.58	0.57

Table 11: Attack performance before and after calibration for non-image datasets w.r.t. GAN training set sizes. **bb**: black-box; **wb**: white-box.

B.5 Comparison to baseline attacks

Table 12 corresponds to Figure 11 in the main paper. Table 13 corresponds to Figure 12 in the main paper.

	PGGAN	WGANGP	DCGAN	VAEGAN
full bb (LOGAN)	0.56	0.57	0.52	0.50
full bb (MC)	0.52	0.52	0.51	0.50
full bb (ours calibrated)	0.54	0.54	0.52	0.51
partial bb (ours calibrated)	0.58	0.63	0.56	0.59
wb (ours calibrated)	0.68	0.66	0.55	0.76
dis (LOGAN)	0.91	0.83	0.83	0.61

Table 12: Comparison of different attacks on CelebA. **bb**: black-box; **wb**: white-box; **dis**: accessible discriminator.

(a) MIMIC-III (WGANGP)								
	64	128	256	512	1024	2048	4096	20k
full bb (LOGAN)	0.98	0.97	0.96	0.94	0.92	0.83	0.65	0.54
full bb (ours calibrated)	1.00	0.99	0.97	0.94	0.89	0.84	0.67	0.56
wb (ours calibrated)	0.98	0.97	0.93	0.90	0.87	0.85	0.75	0.59
dis (LOGAN)	1.00	1.00	1.00	1.00	1.00	1.00	0.99	0.98

(b) MIMIC-III (MEDGAN)								
	64	128	256	512	1024	2048	4096	8192
full bb (LOGAN)	0.45	0.57	0.53	0.52	0.51	0.52	0.50	0.51
full bb (ours calibrated)	0.91	0.71	0.63	0.58	0.55	0.53	0.52	0.51
wb (calibrated)	0.96	0.87	0.81	0.75	0.65	0.62	0.57	0.55
dis (LOGAN)	1.00	0.92	0.96	0.90	0.85	0.90	0.80	0.73

(c) Instagram (WGANGP)									
	64	128	256	512	1024	2048	4096	8192	10k
full bb (LOGAN)	1.00	0.99	0.96	0.91	0.68	0.55	0.58	0.55	0.55
full bb (calibrated)	1.00	1.00	0.98	0.91	0.80	0.72	0.65	0.57	0.56
wb (calibrated)	1.00	1.00	0.98	0.92	0.79	0.73	0.67	0.58	0.57
dis (LOGAN)	1.00	1.00	1.00	1.00	1.00	1.00	0.98	0.96	0.93

Table 13: Comparison of different attacks on the other two non-image datasets w.r.t. GAN training set size. **bb**: black-box; **wb**: white-box; **dis**: accessible discriminator.

B.6 Defense

Table 14 corresponds to Figure 13 in the main paper. Table 15 corresponds to Figure 14 in the main paper.

	full black-box	partial black-box	white-box
w/o DP	0.54	0.58	0.68
w/ DP	0.53	0.56	0.59

Table 14: Attack performance against PGGAN on CelebA with or without DP defense.

	64	128	256	512	1024	2048	4096
white-box w/o DP	1.00	1.00	1.00	0.99	0.95	0.83	0.62
white-box w/ DP	1.00	1.00	0.99	0.98	0.90	0.70	0.56
full black-box w/o DP	1.00	1.00	1.00	0.99	0.95	0.79	0.57
full black-box w/ DP	1.00	1.00	0.99	0.98	0.89	0.68	0.53

Table 15: Attack performance against PGGAN on CelebA with or without DP defense, w.r.t. GAN training set size.

C Qualitative results

Given query samples x , we show their reconstruction copies $R(x|\mathcal{G}_v)$ and $R(x|\mathcal{G}_r)$ obtained in our white-box attack.



(a) Query (real) images



(b) PPGAN victim model reconstruction



(c) PPGAN (w/ DP) victim model reconstruction



(d) PPGAN reference model reconstruction



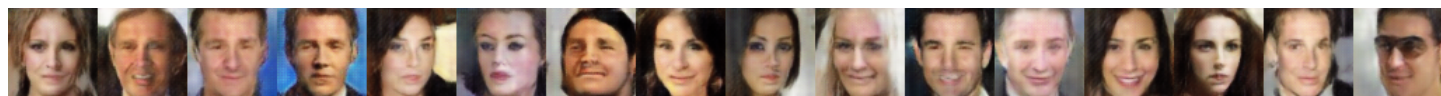
(e) WGANGP victim model reconstruction



(f) WGANGP reference model reconstruction



(g) DCGAN victim model reconstruction



(h) DCGAN reference model reconstruction



(i) VAEGAN victim model reconstruction



(j) VAEGAN reference model reconstruction

Figure 15: Reconstruction of query samples x that are in the training set, i.e., $x \in D_{\text{train}}$.



(a) Query (real) images



(b) PPGAN victim model reconstruction



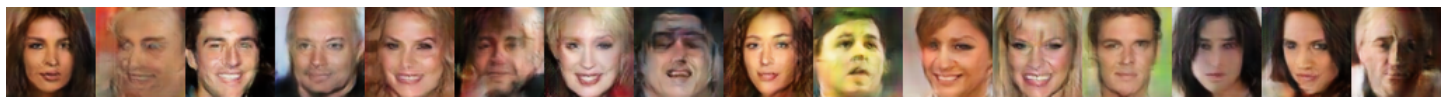
(c) PPGAN (w/ DP) victim model reconstruction



(d) PPGAN reference model reconstruction



(e) WGAN-GP victim model reconstruction



(f) WGAN-GP reference model reconstruction



(g) DCGAN victim model reconstruction



(h) DCGAN reference model reconstruction



(i) VAEGAN victim model reconstruction



(j) VAEGAN reference model reconstruction

Figure 16: Reconstruction of query samples x that are **not** in the training set, i.e., $x \notin D_{\text{train}}$.